

# The Geometric Distance and Proper Motion of the Triangulum Galaxy (M33)

Andreas Brunthaler,<sup>1,2</sup> Mark J. Reid,<sup>3</sup> Heino Falcke,<sup>4,5</sup>  
Lincoln J. Greenhill,<sup>3</sup> Christian Henkel<sup>1</sup>

<sup>1</sup>Max-Planck-Institut für Radioastronomie, Auf dem Hügel 69, 53121 Bonn, Germany

<sup>2</sup>Joint Institute for VLBI in Europe, Postbus 2, 7990 AA Dwingeloo, The Netherlands

<sup>3</sup>Harvard-Smithsonian Center for Astrophysics, 60 Garden Street, Cambridge, MA 02138, USA

<sup>4</sup>ASTRON, Postbus 2, 7990 AA Dwingeloo, The Netherlands

<sup>5</sup>Department of Astrophysics, Radboud Universiteit Nijmegen,  
Postbus 9010, 6500 GL Nijmegen, The Netherlands

**We measured the angular rotation and proper motion of the Triangulum Galaxy (M33) with the Very Long Baseline Array by observing two H<sub>2</sub>O masers on opposite sides of the galaxy. By comparing the angular rotation rate with the inclination and rotation speed, we obtained a distance of  $730 \pm 168$  kiloparsecs. This distance is consistent with the most recent Cepheid distance measurement. M33 is moving with a velocity of  $190 \pm 59$  km s<sup>-1</sup> relative to the Milky Way. These measurements promise a new method to determine dynamical models for the Local Group and the mass and dark matter halos of M31, M33 and the Milky Way.**

Measuring the proper motion and geometric distances of nearby galaxies has been a long-standing problem. As part of a famous debate about the nature of galaxies, van Maanen – an experienced observer – claimed in 1923 to have measured a large proper motion and angular

rotation rate for the Triangulum Galaxy (M33) on photographic plates separated by 12 years (1). This was proven wrong by Hubble through the discovery of Cepheids in M33 that showed a large distance (2). This pushed the detection of galaxy proper motions beyond the capabilities of past experiments. Yet, galaxy proper motions are important for many astrophysical issues, of which two are addressed in this report.

First, measuring accurate distances is of great importance to all fields of astrophysics, from stellar astronomy to cosmology. The calibration of most standard candles used for measuring extragalactic distances is tied directly or indirectly to the distance to one galaxy, the Large Magellanic Cloud (LMC), which remains controversial (3, 4). Hence, it is important to obtain geometric distances to nearby galaxies in which well understood standard candles can be studied. This allows independent calibration and verification of the extragalactic distance scale.

Another important issue is the distribution of luminous and dark matter in the local universe. The problem when trying to derive the gravitational potential of the Local Group of galaxies (5) is that usually only radial velocities are known from the Doppler effect and statistical approaches have to be used (6, 7). The proper motions of some nearby galaxies in the Milky Way subgroup have been obtained from comparing historic photographic plates (8, 9), but a confirmation of these measurements will require decades. With Very Long Baseline Interferometry (VLBI) and phase-referencing techniques, the proper motions for galaxies within the Local Group, on scales of tens of microarcseconds per year, can now be measured. The most suitable strong and compact radio sources in the Local Group for such a VLBI experiment are the strong H<sub>2</sub>O masers in M33 and in the galaxy IC 10 (10, 11).

We observed two HII regions (12) in M33 with known H<sub>2</sub>O maser activity – M33/19 and IC 133 – with the NRAO Very Long Baseline Array (VLBA) eight times between March 2001 and January 2004. M33/19 is located in the south eastern part of M33, whereas IC 133 is located in the north east of M33 (*Fig.1*). Our observations are grouped into four epochs, each compris-

Table 1: Details of the observations: Observing date, observation length  $t_{obs}$ , beam size  $\theta$  and position angle  $PA$ .

Epoch	Date	$t_{obs}[h]$	$\theta$ [mas]	$PA[^\circ]$
I	2001/03/27	10	$0.88 \times 0.41$	164
I	2001/04/05	10	$0.86 \times 0.39$	169
II	2002/01/28	10	$0.62 \times 0.33$	176
II	2002/02/03	10	$0.71 \times 0.33$	175
III	2002/10/30	10	$0.87 \times 0.38$	171
III	2002/11/12	10	$0.84 \times 0.36$	165
IV	2003/12/14	12	$0.85 \times 0.36$	159
IV	2004/01/08	12	$1.15 \times 0.47$	164

ing two closely spaced observations to enable assessment of overall accuracy and systematic errors (Table 1). The separations of the two observations within each epoch were large enough that the weather conditions were uncorrelated, but small enough that changes in the positions were negligible during this time.

We observed four 8 MHz bands, in dual circular polarization. The 128 spectral channels in each band yielded a channel spacing of 62.5 kHz, equivalent to  $0.84 \text{ km s}^{-1}$ , and covered a velocity range of  $107 \text{ km s}^{-1}$ . The observations involved rapid switching between the phase-calibrator J0137+312, which is a compact background source with continuum emission, and the target sources IC 133 and M33/19 in the sequence J0137+312 – IC 133 – J0137+312 – M33/19 – J0137+312. With source changes every 30 seconds, an integration time of 22 seconds was achieved. The background source was unresolved in all epochs and was assumed to be stationary on the sky. Because J0137+312 was separated by only  $1^\circ$  on the sky from the masers, we obtained a precise angular separation measurement for all sources.

The data were edited and calibrated with standard techniques in the Astronomical Image Processing System (AIPS) as well as zenith delay corrections (13). The masers in IC 133 and M33/19 were imaged with standard techniques in AIPS. In IC 133, we detected 29 distinct

emission features in position and the spatial distribution was very similar to earlier observations (10, 14, 15). All components were unresolved. In M33/19, we detected eight maser features. Two features were separated by less than a beam size and blended together. These two features were fit by two elliptical Gaussian components simultaneously. All other features were fit by a single elliptical Gaussian component.

The maser emission in M33/19 and IC 133 is variable on time scales less than 1 year. Between the epochs, new maser features appeared and others disappeared. However, we were able to detect and follow the motions of four features in M33/19 and six features in IC 133 over all four epochs. The feature identification was based on the positions and radial velocities of the maser emission. Each feature was usually detected in several frequency channels. A rectilinear motion was fit to each maser feature in each velocity channel separately. We discarded fits with reduced  $\chi^2$  larger than 3 as they are likely affected by blending or component misidentification. All features showed consistent motions within their errors ( $2\sigma$ ). The accuracy and number of measured motions was not adequate to model the internal dynamics of the IC133 and M33/19 regions (such as outflow) as was done in earlier observations (15, 10).

We then calculated the variance weighted average of all motions. This yielded an average motion of the maser features in M33/19 of  $35.5 \pm 2.7 \mu\text{as year}^{-1}$  in right ascension and  $-12.5 \pm 6.3 \mu\text{as year}^{-1}$  in declination relative to the background source. For IC 133 we get an average motion of  $4.7 \pm 3.2 \mu\text{as year}^{-1}$  in right ascension and  $-14.1 \pm 6.4 \mu\text{as year}^{-1}$  in declination.

We also calculated the average position of all maser features for each observation (Fig. 2 and 3). We used the individual fits for each maser feature to remove a constant position offset for each maser feature. We used the position offsets at the time 2002.627, which is in the middle of our observations. We then calculated the variance weighted average of the positions of all detected features. A fit of a rectilinear motion to these average positions yielded motions of  $37 \pm 5 \mu\text{as year}^{-1}$  in right ascension and  $-13 \pm 6 \mu\text{as year}^{-1}$  in declination for M33/19. For

IC 133 we obtained a motion of  $3 \pm 3 \mu\text{as year}^{-1}$  in right ascension and  $-13 \pm 10 \mu\text{as year}^{-1}$  in declination. This is consistent with the variance weighted average of all maser feature motions and suggests that the systematic internal motions within the two regions (such as outflow) are probably not a substantial source of bias. The difference in the maser position of the two closely spaced observations within each epoch was used to estimate the accuracy of the position measurements. The average position error over the four epochs was  $7.7 \mu\text{as}$  in right ascension and  $9.8 \mu\text{as}$  in declination.

The relative motions between M33/19 and IC 133 are independent of the proper motion of M33 and any contribution from the rotation of the Milky Way. Knowing the rotation curve and inclination of the galactic disk we can predict the relative angular motion of the two masing regions as a function of distance. The rotation of the HI gas in M33 has been measured and the measured velocities were fit with a tilted-ring model (16). We used this model of the rotation of M33 to calculate the expected transverse velocities of M33/19 and IC 133. For M33/19, we expect a motion of  $42.4 \text{ km s}^{-1}$  in right ascension and  $-39.6 \text{ km s}^{-1}$  in declination. For IC 133 we expect  $-64.0 \text{ km s}^{-1}$  in right ascension and  $-74.6 \text{ km s}^{-1}$  in declination. This gives a relative motion of  $106.4 \text{ km s}^{-1}$  in right ascension and  $35 \text{ km s}^{-1}$  in declination between the two regions of maser activity.

The radial velocities of the H<sub>2</sub>O masers in M33/19 and IC 133 and the HI gas at the same positions agree ( $< 10 \text{ km s}^{-1}$ ). This suggests that the maser sources are moving with the HI gas in the galaxy. However, although the rotation model and the radial velocity of the HI gas at the position of IC 133 is also consistent ( $< 5 \text{ km s}^{-1}$ ), there is a difference of  $\sim 15 \text{ km s}^{-1}$  at the position of M33/19. This indicates the presence of another tilt in the disk that is not covered by the model. Because of this uncertainty in the rotation model, we conservatively assume a systematic error of  $20 \text{ km s}^{-1}$  in each velocity component for the relative velocity of the two maser components.

Comparing the measured angular motion of  $30.8 \pm 4 \mu\text{as year}^{-1}$  in right ascension with the expected linear motion of  $106 \pm 20 \text{ km s}^{-1}$ , one gets a geometric distance of

$$D = 730 \pm 100 \pm 135 \text{ kpc},$$

where the first error indicates the statistical error from the proper motion measurements while the second error is the systematic error from the rotation model. After less than three years of observations, the uncertainty in the distance estimate is dominated by the uncertainty of the rotation model of M33.

Within the errors the geometric distance of  $730 \pm 100 \pm 135 \text{ kpc}$  is consistent with recent Cepheid and tip of the red giant branch (TRGB) distances of  $802 \pm 51 \text{ kpc}$  and  $794 \pm 23 \text{ kpc}$  respectively (17, 18). It also agrees with a geometric distance estimate of  $800 \pm 180 \text{ kpc}$  (10).

The observed proper motion  $\vec{v}_{prop}$  of a maser (e.g., M33/19 or IC 133) in M33 can be decomposed into three components  $\vec{v}_{prop} = \vec{v}_{rot} + \vec{v}_{\odot} + \vec{v}_{M33}$ . Here  $\vec{v}_{rot}$  is the motion of the maser due to the internal galactic rotation in M33 and  $\vec{v}_{\odot}$  is the apparent motion of M33 caused by the rotation of the Sun around the Galactic center. The last contribution,  $\vec{v}_{M33}$ , is the proper motion of M33 relative to the Milky Way.

The motion of the Sun can be decomposed into a circular motion of the local standard of rest (LSR) and the peculiar motion of the Sun. The peculiar motion of the Sun has been determined from Hipparcos data (19) to be  $U_0 = 10.00 \pm 0.36 \text{ km s}^{-1}$  (radially inwards),  $V_0 = 5.25 \pm 0.62 \text{ km s}^{-1}$  (in the direction of Galactic rotation) and  $W_0 = 7.17 \pm 0.38 \text{ km s}^{-1}$  (vertically upwards). The IAU adopted LSR moves with a velocity of  $220 \text{ km s}^{-1}$  towards a Galactic longitude of  $l = 90^\circ$  and latitude of  $b = 0^\circ$  (20). New VLBI measurements of the proper motion of Sgr A\*, the compact radio source at the Galactic center, indicate a slightly higher circular velocity of the LSR of  $236 \pm 15 \text{ km s}^{-1}$ , for a distance of the Sun from the Galactic center  $R_0 = 8 \text{ kpc}$ , where the

uncertainty is dominated by the uncertainty in the distance to the Galactic center (13). Using a LSR velocity of  $236 \pm 15 \text{ km s}^{-1}$  plus the peculiar velocity of the Sun from (19), the motion of the Sun causes an apparent proper motion of  $\dot{\alpha}_{\odot} = 52.5 \pm 3.3 \mu\text{as year}^{-1}$  in right ascension and  $\dot{\delta}_{\odot} = -37.7 \pm 2.4 \mu\text{as year}^{-1}$  in declination, assuming a distance of 730 kpc and the Galactic coordinates of M33 ( $l = 133.6^{\circ}$ ,  $b = -31.3^{\circ}$ ).

Using the rotation model of (16), the contribution from the rotation of M33 (for IC 133) is  $\dot{\alpha}_{rot} = -18.5 \pm 6 \mu\text{as year}^{-1}$  in right ascension and  $\dot{\delta}_{rot} = -21.6 \pm 6 \mu\text{as year}^{-1}$  in declination. Here, we assumed again an uncertainty of  $20 \text{ km s}^{-1}$  for the rotation velocity and a distance of 730 kpc. Combining these velocity vectors, we get the proper motion of M33:

$$\begin{aligned}\dot{\alpha}_{M33} &= \dot{\alpha}_{prop} - \dot{\alpha}_{rot} - \dot{\alpha}_{\odot} \\ &= (4.7 \pm 3.2 + 18.5 \pm 6 - 52.5 \pm 3.3) \frac{\mu\text{as}}{\text{year}} \\ &= -29.3 \pm 7.6 \frac{\mu\text{as}}{\text{year}} = -101 \pm 35 \frac{\text{km}}{\text{s}}\end{aligned}$$

and

$$\begin{aligned}\dot{\delta}_{M33} &= \dot{\delta}_{prop} - \dot{\delta}_{rot} - \dot{\delta}_{\odot} \\ &= (-14.1 \pm 6.4 + 21.6 \pm 6 + 37.7 \pm 2.4) \frac{\mu\text{as}}{\text{year}} \\ &= 45.2 \pm 9.1 \frac{\mu\text{as}}{\text{year}} = 156 \pm 47 \frac{\text{km}}{\text{s}}.\end{aligned}$$

The transverse velocity changes by less than  $5 \text{ km s}^{-1}$  if we use the TRGB distance of  $794 \pm 23 \text{ kpc}$  (18) for this analysis. Finally, the systemic radial velocity of M33 is  $-179 \text{ km s}^{-1}$  (16). The radial component of the rotation of the Milky Way towards M33 is  $-140 \pm 9 \text{ km s}^{-1}$ . Hence, M33 is moving with  $-39 \pm 9 \text{ km s}^{-1}$  towards the Milky Way. This gives now the three dimensional velocity vector of M33 (Fig.4). The total velocity of M33 relative to the Milky Way is  $190 \pm 59 \text{ km s}^{-1}$ .

For Andromeda (M31), only one component of the three-dimensional velocity vector is

known, the radial velocity of  $116 \text{ km s}^{-1}$  ( $301 \text{ km s}^{-1}$  systemic velocity minus  $185 \text{ km s}^{-1}$  contribution from solar motion) towards the Milky Way. However, the Milky Way is possibly falling towards M31, because there are no other large galaxies in the Local Group to generate angular momentum through tidal torques (21). Following this argument, we assume a proper motion of 0 for M31. The geometry of the Andromeda subgroup depends on the relative distance between M31 and M33. Thus, it is crucial to use distances for the two galaxies that have similar systematic errors, and we used the TRGB distances to M33 and M31 (18, 22). Then the angle between the velocity vector of M33 relative to M31 and the vector pointing from M33 towards M31 was  $30^\circ \pm 15^\circ$ . For an angle of  $30^\circ$ , only elliptical orbits with eccentricities of  $e > 0.88$  are allowed. For the largest allowed angle of  $45^\circ$ , the eccentricities are restricted to  $e > 0.7$ . This eccentricity limit weakens if the proper motion of M31 is non-negligible and, for a motion of  $> 150 \text{ km s}^{-1}$ , any eccentricity is allowed.

If M33 is bound to M31, then the relative velocity of the two galaxies must be smaller than the escape velocity. This gives – for a zero proper motion of M31 – a lower limit for the mass of M31 of  $1.2 \times 10^{12} M_\odot$ . A substantial proper motion of M31 could reduce or increase the relative velocity and the lower mass limit of M31. On the other hand, the dynamical friction of M31 on M33 indicates that M31 cannot have a very massive halo of more than  $\sim 10^{12} M_\odot$  unless the orbit of M33 has a low eccentricity. Otherwise, the dynamical friction would have led to a decay of the orbit of M33 (23). This agrees with a recent estimates of  $12.3_{-6}^{+18} \times 10^{11} M_\odot$  derived from the three-dimensional positions and radial velocities of its satellite galaxies (24).

More than 80 years after van Maanen’s observation, we have measured the rotation and proper motion of M33. These measurements provide a method to determine dynamical models for the Local Group and the mass and dark matter halo of Andromeda and the Milky Way.



## References and Notes

1. A. van Maanen, ApJ **57**, 264 (1923).
2. E. P. Hubble, ApJ **63**, 236 (1926).
3. W. L. Freedman, *et al.*, ApJ **553**, 47 (2001).
4. A. Udalski, *et al.*, ApJ **509**, L25 (1998).
5. The Local Group is a small galaxy group in the local universe that includes the Milky Way, M31, M33 and 30 – 40 other small galaxies within a radius of  $\sim 1$  Mpc.
6. F. D. A. Hartwick, W. L. W. Sargent, ApJ **221**, 512 (1978).
7. A. S. Kulessa, D. Lynden-Bell, MNRAS **255**, 105 (1992).
8. B. F. Jones, A. R. Klemola, D. N. C. Lin, AJ **107**, 1333 (1994).
9. A. E. Schweitzer, K. M. Cudworth, S. R. Majewski, N. B. Suntzeff, AJ **110**, 2747+ (1995).
10. A. L. Argon, *et al.*, ApJ **615**, 702 (2004).
11. A. L. Argon, *et al.*, ApJ **422**, 586 (1994).
12. F. P. Israel, P. C. van der Kruit, A&A **32**, 363 (1974).
13. M. J. Reid, A. Brunthaler, ApJ **616**, 872 (2004).
14. L. J. Greenhill, *et al.*, ApJ **364**, 513 (1990).
15. L. J. Greenhill, J. M. Moran, M. J. Reid, K. M. Menten, H. Hirabayashi, ApJ **406**, 482 (1993).
16. E. Corbelli, S. E. Schneider, ApJ **479**, 244 (1997).

17. M. G. Lee, M. Kim, A. Sarajedini, D. Geisler, W. Gieren, *ApJ* **565**, 959 (2002).
18. A. W. McConnachie, *et al.*, *MNRAS* **350**, 243 (2004).
19. W. Dehnen, J. J. Binney, *MNRAS* **298**, 387 (1998).
20. F. J. Kerr, D. Lynden-Bell, *MNRAS* **221**, 1023 (1986).
21. F. D. Kahn, L. Woltjer, *ApJ* **130**, 705 (1959).
22. A. W. McConnachie, *et al.*, *MNRAS* **356**, 979 (2005).
23. S. T. Gottesman, J. H. Hunter, V. Boonyasait, *MNRAS* **337**, 34 (2002).
24. N. W. Evans, M. I. Wilkinson, *MNRAS* **316**, 929 (2000).
25. S. van den Bergh, *A&A Rev.* **9**, 273 (1999).
26. The VLBA is operated by the National Radio Astronomy Observatory (NRAO). The National Radio Astronomy Observatory is a facility of the National Science Foundation operated under cooperative agreement by Associated Universities, Inc.

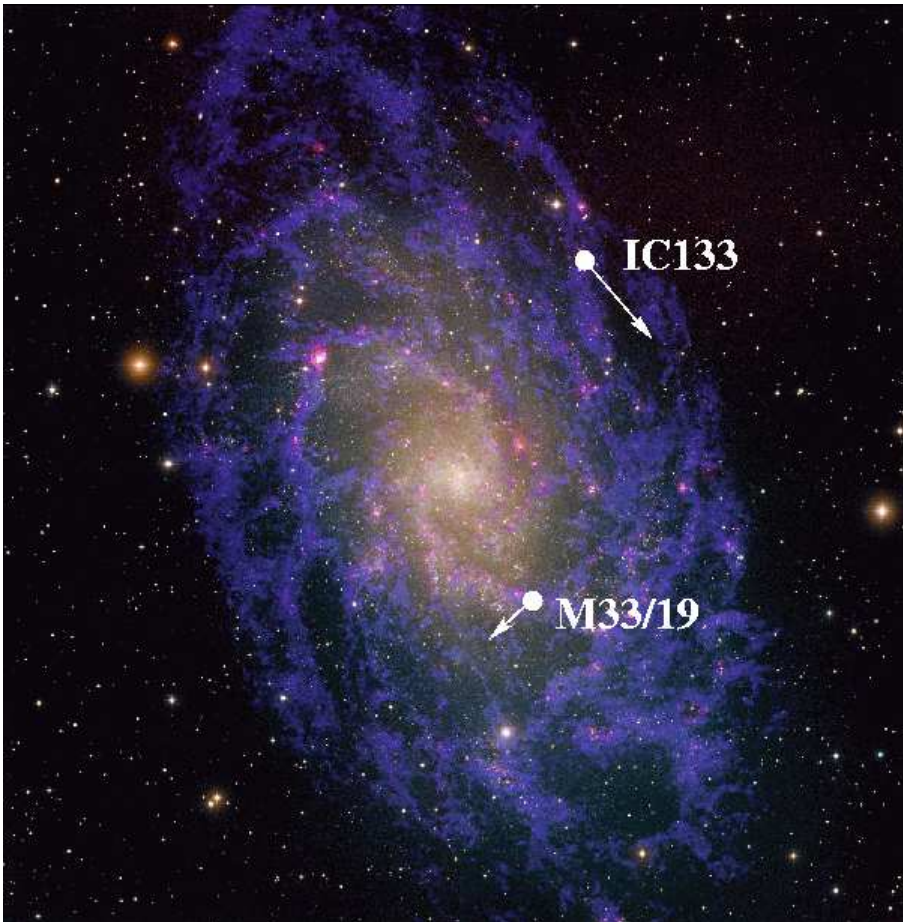


Figure 1: The positions of two regions of maser activity in M33. Predicted motions due to rotation of the HI disk are also shown. Image courtesy of Travis Rector (NRAO/AUI/NSF and NOAO/AURA/NSF), David Thilker (NRAO/AUI/NSF) and Robert Braun (ASTRON).

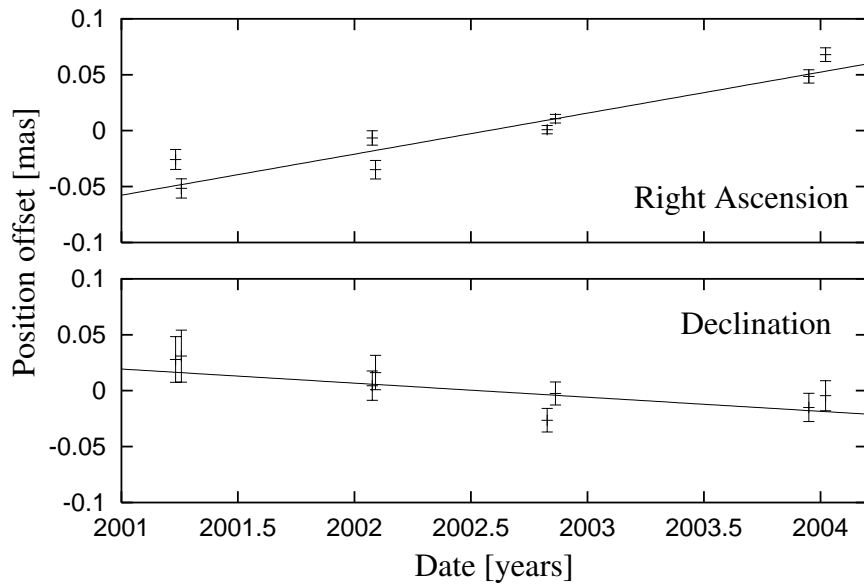


Figure 2: Average position of the maser M33/19 in (top) right ascension and (bottom) declination relative to a background source.

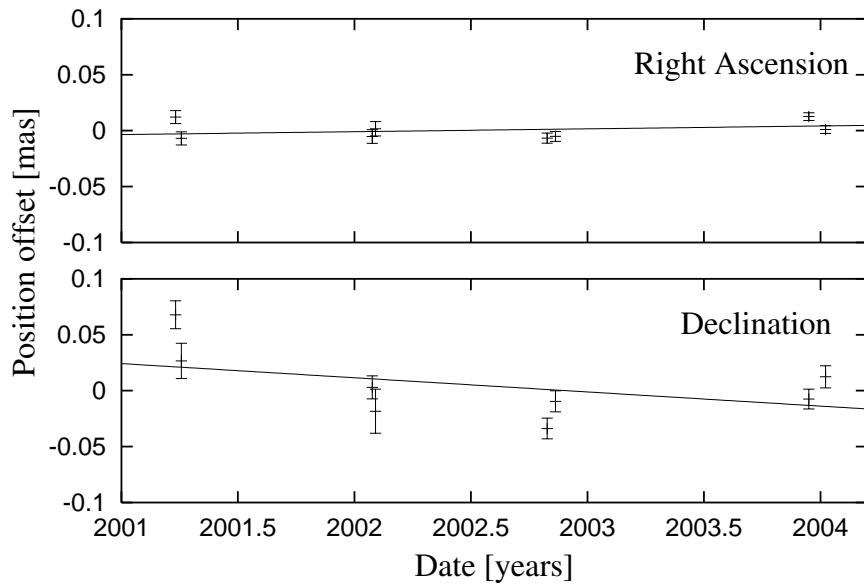


Figure 3: Average position of the masers in (top) IC 133 in right ascension and (bottom) declination relative to a background source.

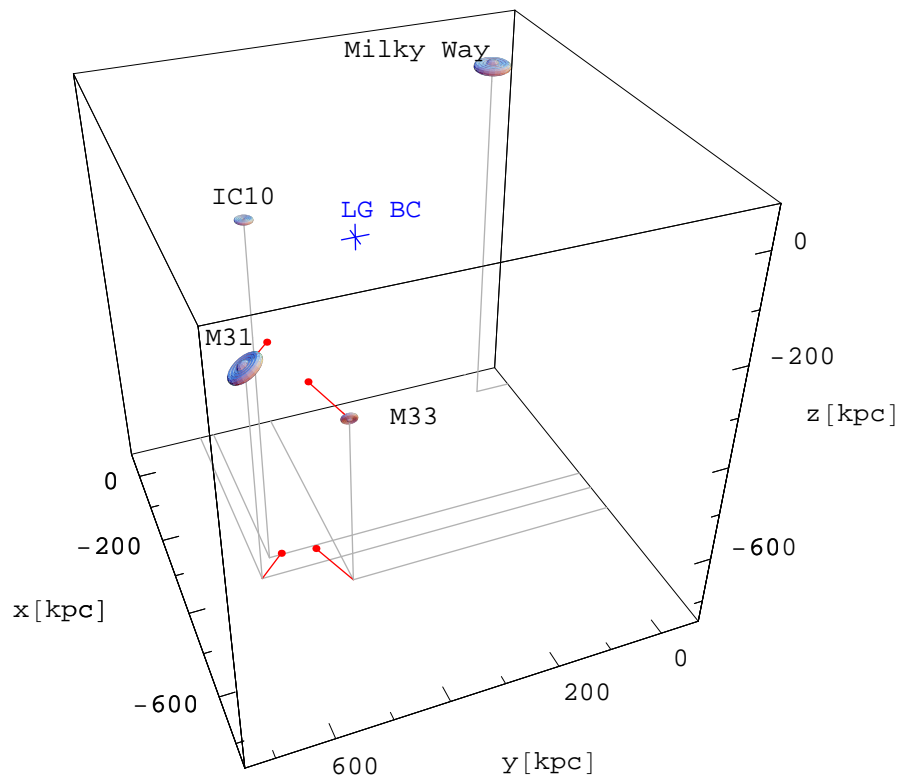


Figure 4: Schematic view of the Local Group with the space velocity of M33 and the radial velocity of M31. The blue cross marks the position of the Local Group Barycenter (LG BC) (25).